Numerical Investigation of RT25HC Phase-Change Material for Passive Cooling of Photovoltaic Modules

Muhammad Ehtisham Khan, Muhammad Saad Rehan, Khurshid Ahmad, Muhammad Hassan*
U.S.-Pakistan Center for Advanced Studies in Energy, University of Engineering and Technology, Peshawar 25000, Pakistan.
*Corresponding author: muhammad.hassan@uetpeshawar.edu.pk
Received: 29-04-2026, Received in Revised form: 25-05-2026, Accepted: 24-06-2026, Published: 30-06-2026

Abstract

High temperatures degrade PV module performance, yet effective thermal management remains challenging in warm climates. This study numerically investigates passive cooling of a PV module by integrating RT25HC phase change material (PCM) on its back surface, using the commercial CFD code ANSYS Fluent. The enthalpy-porosity approach captured both sensible and latent heat storage within the PCM. Results show that the PV–PCM configuration limits the maximum PV temperature to approximately 315 K, compared with approximately 348 K for the PV-only configuration under the investigated operating condition. As the PCM melts, natural convection within the liquid phase aids internal heat redistribution. This thermal regulation increased the estimated electrical efficiency from 15.59% for the PV-only configuration to 18.56% for the PV–PCM configuration, an absolute improvement of 2.97% and a relative improvement of approximately 19.1%. Passive cooling with PCMs like RT25HC offers an effective and low-maintenance solution for enhancing PV performance in hot climates.
Keywords: Photovoltaic module, Phase change material (RT25HC), Passive cooling, CFD simulation, Thermal regulation.

Introduction

The recent rise in the use of fossil fuels over the last several decades has resulted in resource depletion, but it has also caused an increase in greenhouse gas emissions, which have caused global warming and climate change to a significant degree [1, 2]. To address these fears, renewable energy technologies have been given much consideration as the eco-friendly option for energy security on a long-term basis [3]. Solar energy is one of the alternatives that can be highlighted as the most suitable option because of its abundance, environmental friendliness, and scalability to various uses [4]. Consequently, photovoltaic (PV) technologies have grown steadily worldwide, with installed capacity increasing significantly in recent years.

Solar photovoltaic systems convert solar radiation directly into direct current electricity, which can be converted to alternating current for use at home or in industry. They are relatively easy to install, not demanding in terms of maintenance and have a long operational span, which renders them appealing when it comes to grid-connected applications as well as standalone ones [5-7]. Over the past decade, the world PV market has increased at a rate of more than 50 per annum on average [8]. And even with these benefits, traditional PV modules continue to achieve relatively small electrical efficiencies, generally in the 9-17 percent range under normal conditions [9]. Another major cause of this weakness is the temperature sensitivity of PV cell performance.

High operating temperature adversely affects semiconductor properties, causing a voltage drop and reduced total power output. Moreover, high temperatures over long periods lead to degradation of materials, which adds to the reduction in efficiency of about 0.5-1.0 per year, with respect to environmental and installation conditions [10, 11]. The thermal performance of a PV system is dependent on ambient temperature, solar irradiance, wind speed, tilt angle, and the construction of the modules [12, 13]. Therefore, proper thermal management has recently become a significant research interest for enhancing performance and durability.

The different methods of cooling have been explored to reduce the losses due to temperature. Such strategies are classified as active or passive systems in general [14-17]. Active cooling systems, such as forced air or liquid circulation, can achieve large temperature reductions, but they require more energy and are more complex and expensive. Passive cooling strategies, in turn, do not require power and rely on heat-dissipation processes built into the module design. They are usually less complex, but their effectiveness depends heavily on material choice and setup.

A good passive method is the employment of phase change materials (PCMs) on the back of the PV modules [18]. PCMs can absorb and release large amounts of thermal energy by transitioning between phases. The PCM can store large amounts of latent heat at almost constant temperature during melting or solidification, unlike conventional materials that store the heat mainly as sensible heat [19]. This makes them especially suitable for stabilizing PV operating temperatures under high solar irradiation. Figure 1 shows how the latent heat and sensible heat are controlled in terms of temperature during the phase changes of PCM [20].

PCM-based systems (PV–PCM), when combined with photovoltaic modules, also strive to control cell temperature through transiently absorbing excess thermal energy. The PV/PCM designs are much simpler in design, do not need any circulating fluids as needed in conventional PV/T systems, and have lower maintenance needs as well as no auxiliary power consumption [21]. The common solar PV system transforms the incident solar radiation into electrical power, which is subsequently used in inverters to supply the grid or load, and this is shown in Figure 2 [22].

http://dx.doi.org/10.24949/njes.v19i1.956

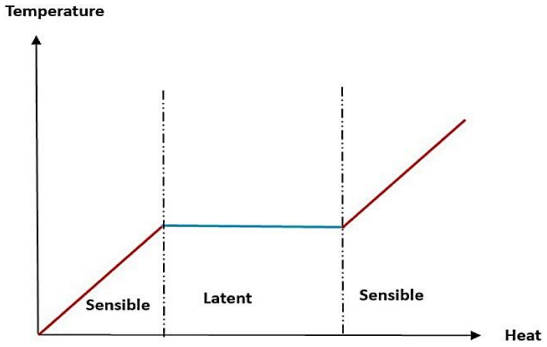

Figure 1: Temperature variation during PCM phase change.

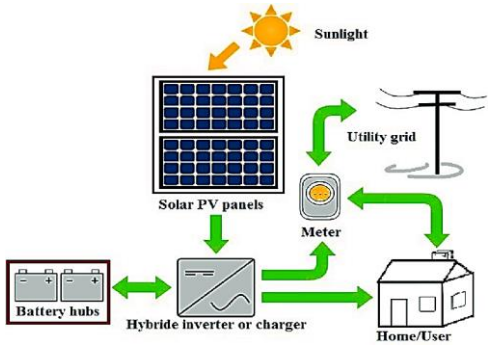

Figure 2: Schematic diagram of a typical solar PV system

Based on these points, this research is a numerical study of the thermal characteristics of a PV module with a paraffin-based PCM (RT25HC), performed via numerical simulation. The aim is to examine the PCM layer's temperature-regulation capacity and its effect on overall thermal performance under a constant solar load.

Materials and Methods

Physical System Description

The layout of the PV-PCM system that is considered in the current study is shown in Figure 3. The module is tilted at an incline angle θ relative to the horizontal plane. The photovoltaic cell length is 132 mm, with the overall structure being made up of a series of multiple layered components. The system consists of an EVA encapsulant layer, a front glass cover, a silicon solar cell, a back EVA cover, and an aluminum sheet, in that order.

In the PV-PCM setup, an extra aluminum plate is fixed to the bottom of the conventional PV layers to hold the PCM layer. The PCM (RT25HC), a paraffin-based compound, is placed in contact with this aluminum substrate to increase heat conduction from the PV module to the storage medium. Table 1 shows the thermophysical properties and thicknesses of the PV and aluminum plates.

The PCM layer thickness in the vertical (y) direction is 20 mm. The bottom and side boundaries of the computational domain were treated as adiabatic, while a uniform solar heat flux of 1000 W/m² was applied at the top surface. This simplified boundary condition was adopted to focus on the thermal-storage and melting behavior of the PV–PCM configuration. The assumption neglects rear and side heat losses to the ambient environment and is therefore recognized as a limitation of the present numerical model. No separate optical transmission–absorption model was implemented for the glass and EVA layers. This approach provides a simplified representation of the solar thermal input and allows the thermal response and PCM melting behavior to be investigated under a constant irradiance condition. This setup enables study of heat transfer in the layered structure and the PCM's thermal storage behavior during operation.

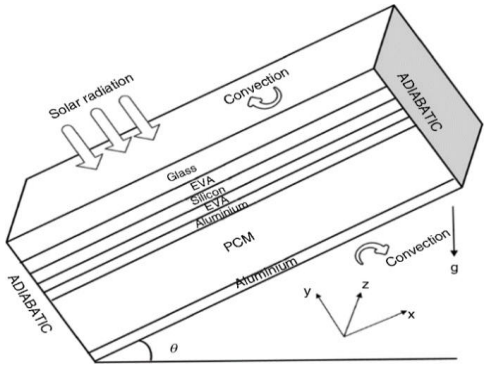

Figure 3: Description of the PV-PCM system

Table 1: Thermophysical properties and thicknesses of PV module layers and aluminum backing [23]

Material	Density (kg/m³)	Specific Heat (J/kg·K)	Thermal Conductivity (W/m·K)	Thickness (mm)
Glass	3000	510	1.8	3
EVA (Ethylene Vinyl Acetate)	960	2090	0.35	0.5
Silicon	2320	677	148	0.3
Aluminum	2675	903	211	2

Thermophysical Properties of Phase Change Material

The PCM chosen to be used in this study is RT25HC, which is a commercial product made of paraffin, produced by Rubitherm. RT is the manufacturer's abbreviation, and 25HC indicates the nominal melting-temperature range and increased latent heat storage capacity. RT25HC has a comparatively higher latent heat in a relatively narrow phase-transition range than conventional RT materials.

NUST Journal of Engineering Sciences (NJES) is licensed under a Creative Commons Attribution 4.0 International License.

When solar radiation heats the PV surface, conduction in the main layer transfers thermal energy to the PCM region. The PCM temperature reaches a melting range, triggering phase transition and latent heat uptake that limits further temperature increases. The stored heat builds up and is slowly released during periods of low solar intensity as the PCM solidifies.

Table 2 presents the thermophysical properties of RT25HC used in the numerical model, while Table 3 summarizes the dimensions of the PV–PCM components implemented in ANSYS. These properties were introduced in the solver for the solid and liquid phases to accurately reflect phase-transition behavior.

Table 2: Thermophysical properties and thicknesses of PV module layers and aluminum backing

Property	**RT25HC**
Density (kg/m³)	785 (solid) – 749 (liquid)
Specific Heat Capacity (J/kg·K)	1800 (solid) – 2400 (liquid)
Thermal Conductivity (W/m·K)	0.18 (solid) – 0.19 (liquid)
Latent Heat (J/kg)	232,000
Viscosity (Pa·s)	0.001798
Thermal Expansion Coefficient (K^{-1})	0.001

Simulation Assumptions

The following assumptions were made to make the numerical analysis manageable and still physically relevant:

- The molten PCM behaves as an incompressible Newtonian fluid.
- All PV layers are homogeneous and isotropic with uniform thickness.
- Heat transfer within the PCM occurs through conduction and natural convection.
- Solar radiation is uniformly distributed across the top surface of the PV module.
- Thermal contact resistance between adjacent layers is negligible.
- Environmental effects such as dust deposition and rainfall are not considered.
- Electrical resistive losses within the PV cell are excluded from the thermal model.

These assumptions simplify the computational model and do not significantly affect the interpretation of thermal behavior.

Modeling of PV Module

Figure 4 demonstrates that ANSYS DesignModeler was used to create the geometric model. To minimize computational cost while maintaining critical heat-transfer processes across the layered structure, a two-dimensional model was selected.

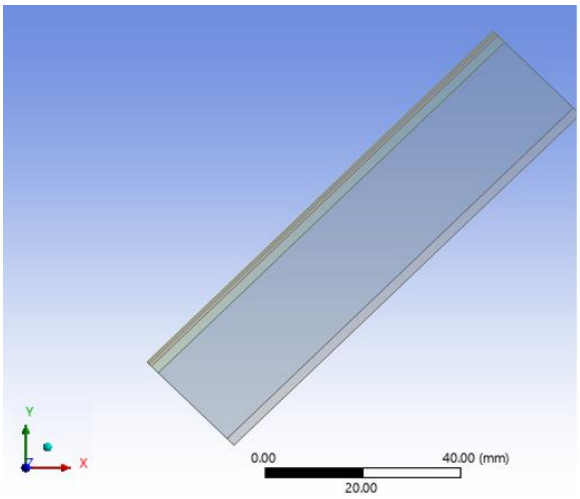

Figure 4: Geometry of PV in ANSYS DesignModeler.

The layers were created in the x-y plane in that order and according to the set dimensional limits. The overall geometry is made up of six separate domains, which are the PV layers, the sheets of aluminum, and the PCM area. Table 3 provides all dimensions of every component applied in ANSYS.

Actual geometric dimensions are also used to ensure the simulation results are representative of a realistic PV-PCM setup.

Table 3: Dimensions of PV–PCM Components in ANSYS [23]

Component	**Length (mm)**	**Thickness (mm)**
EVA Front	120	0.5
Silicon	120	0.3
EVA Back	120	0.5
Aluminium (Top)	120	2
PCM (RT25HC)	120	20
Aluminium (Base)	120	2

Mesh Generation

ANSYS Meshing was used to discretize the computational domain (Figure 5). A primary mesh was created automatically, then refined and further improved to enhance element quality. Special attention was paid to orthogonality (close to 1) and skewness (close to 0), which directly affect numerical stability and convergence. Face meshing was utilized in a structured approach to meshing all domains to maintain a homogeneous distribution of elements. Mesh refinement in the PCM area was particularly important

NUST Journal of Engineering Sciences (NJES) is licensed under a Creative Commons Attribution 4.0 International License.

because it involves phase change and buoyancy-driven flow. Along the vertical edges of the PCM layer, edge sizing with 50 divisions ensured that the temperature gradient and evolution of liquid fractions were accurately captured. For the remaining thin PV layers, element size was calculated based on their typical thickness (2.5×10^{-4} m). This approach produced a balanced mesh, improving solution accuracy while maintaining reasonable computational efficiency. Every surface and body was properly labeled to assign boundary conditions when configuring the solver.



Figure 5: Meshing Model of PV in ANSYS Meshing.

Governing Equations and Solver Setup

ANSYS Fluent was used to perform the transient numerical simulations using a pressure-based solver with the energy equation enabled. The melting and solidification of RT25HC were modeled using the enthalpy-porosity formulation.

For the incompressible flow in the molten PCM region, the continuity equation is expressed as:

$$\frac{\partial u}{\partial x} + \frac{\partial v}{\partial y} = 0 \tag{1}$$

where u and v are the components of velocity in the x and y directions, respectively, and ρ = constant.

The two-dimensional momentum equations account for transient momentum transport, convection, pressure forces, viscous diffusion, and the additional resistance introduced by the mushy region. The governing equations were solved together with the energy equation to describe the coupled heat-transfer and phase-change behavior of the PCM.

Navier–Stokes Equations

The momentum equations for two-dimensional, viscous, incompressible flow can be written as:

X-momentum:

$$\rho\left(\frac{\partial u}{\partial t} + u\frac{\partial u}{\partial x} + v\frac{\partial u}{\partial y}\right) = -\frac{\partial P}{\partial x} + \mu\left(\frac{\partial^2 u}{\partial x^2} + \frac{\partial^2 u}{\partial y^2}\right) + S_x \tag{2}$$

Y-momentum:

$$\rho\left(\frac{\partial v}{\partial t} + u\frac{\partial v}{\partial x} + v\frac{\partial v}{\partial y}\right) = -\frac{\partial P}{\partial y} + \mu\left(\frac{\partial^2 v}{\partial x^2} + \frac{\partial^2 v}{\partial y^2}\right) + S_y \tag{3}$$

where S_x and S_y represent the additional momentum source contributions associated with the phase-change/mushy region and other applicable body-force terms.

These equations describe the transient momentum transport within the molten PCM, while the energy equation accounts for sensible and latent heat transfer during phase change.

Phase Change Modeling

The enthalpy porosity technique was used to model PCM melting. This method uses a liquid fraction in each computational cell, ranging from 0 (solid) to 1 (liquid), so the mushy region can be modeled as a porous medium.

We have the governing equations of mass and momentum, which are given as:

$$\frac{\partial \rho}{\partial t} + \nabla \cdot (\rho \vec{v}) = 0 \tag{4}$$

$$\rho\left(\frac{\partial \vec{v}}{\partial t} + (\vec{v} \cdot \nabla)\vec{v}\right) = -\nabla P + \nabla \cdot (\mu \nabla \vec{v}) + S \tag{5}$$

The model of the porous resistance in the mushy zone is the source term, which is:

$$S_m = A_{mush}\frac{(1-\beta)^2}{\beta^3 + \epsilon}(\vec{v} - \vec{v}_p) \tag{6}$$

Where β is the liquid fraction, A_{mush} is the mushy zone constant, $\vec{v}_p$ is the solid velocity, $\vec{v}$ is the local velocity, and ϵ is a small numerical constant introduced to avoid division by zero.

The energy equation is written as:

$$\frac{\partial}{\partial t}(\rho H) + \nabla \cdot (\rho \vec{v} H) = \nabla \cdot (k \nabla T) + S \tag{7}$$

The total enthalpy Hconsists of sensible and latent components:

$$H = h + \Delta H \tag{8}$$

Sensible enthalpy is defined as:

$$h = h_{ref} + \int_{T_{ref}}^{T} c_p \, dT \tag{9}$$

Where h_{ref} is the reference sensible enthalpy, T_{ref} is the reference temperature, T is the local temperature, and c_p is the specific heat capacity.

Latent heat is expressed as:

$$\Delta H = \beta L \tag{10}$$

The liquid fraction β is determined as:

$$\beta = 0 \text{ if } T \leq T_{solidus} \tag{11}$$

NUST Journal of Engineering Sciences (NJES) is licensed under a Creative Commons Attribution 4.0 International License.

$$\beta = \frac{T - T_{solidus}}{T_{liquidus} - T_{solidus}} \text{ if } T_{solidus} < T < T_{liquidus} \quad (12)$$

$$\beta = 1 \text{ if } T \geq T_{liquidus} \quad (13)$$

The sensible heat absorbed by the PCM can be expressed as:

$$Q_{sensible} = mC_P\Delta T \quad (14)$$

During phase change, additional energy is stored as latent heat. Therefore, the total thermal energy stored in the PCM consists of both sensible and latent contributions and is represented through the total enthalpy formulation used in the enthalpy-porosity model.

The total heat absorbed by the PCM is calculated as:

$$E_{PCM} = m_{PCM}C_{PCM}\Delta T \quad (15)$$

Where m_{PCM}, C_{PCM}, and ΔTdenote PCM mass, specific heat, and temperature change, respectively.

Results and Discussion

A mesh independence analysis was performed to ensure that the numerical predictions were not significantly affected by grid resolution. ANSYS Meshing was used to create four mesh densities: coarse, medium, fine, and very fine. In summary, the grid statistics are presented as shown below [23]:

- Coarse mesh: 5889 nodes and 5700 elements.
- Medium mesh: 10653 nodes and 10400 elements.
- Fine mesh: 16629 nodes and 16320 elements
- Very Fine mesh: 25886 nodes and 25500 elements.

Simulations were conducted in all cases at the same operating conditions (i.e., the same solar heat flux and boundary conditions). The most important comparison parameter was the maximum PV surface temperature, which directly depends on the system's thermal response and is spatially sensitive.

Figure 6 shows the mesh layouts created for the study, while Figure 7 compares the estimated PV temperature across different grid densities. The findings show that the coarse mesh has noticeable deviations, meaning it lacks the resolution to capture temperature gradients fully. Nevertheless, the distinction between fine and very fine meshes is not significant. The temperature curves in the two cases almost coincide throughout the simulation period.

Since the fine and very fine meshes showed insignificant differences, additional refinement was deemed unnecessary. The fine mesh was therefore used in further simulations, as it offers an adequate trade-off between computational cost and numerical accuracy.

To achieve confidence in the numerical approach, the model developed was tested against published data found in the literature [24]. The comparison was based on the temporal change in the PCM liquid fraction throughout the melting process, as this parameter directly reflects the soundness of the enthalpy-porosity formulation adopted in the solver. The comparison of the current numerical results and the reference results is depicted in Figure 8. The general melting patterns, such as the rate of increase of the liquid fraction and the course of complete melting, are in close agreement. The forecast curve trend matches the literature over the entire simulation period.

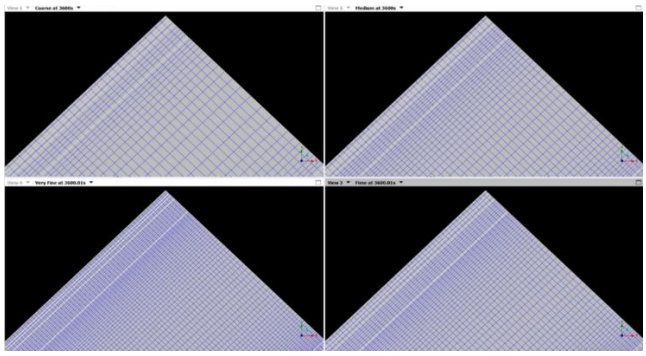

Figure 6: Coarse, Medium, Fine and very fine grids in ANSYS Meshing

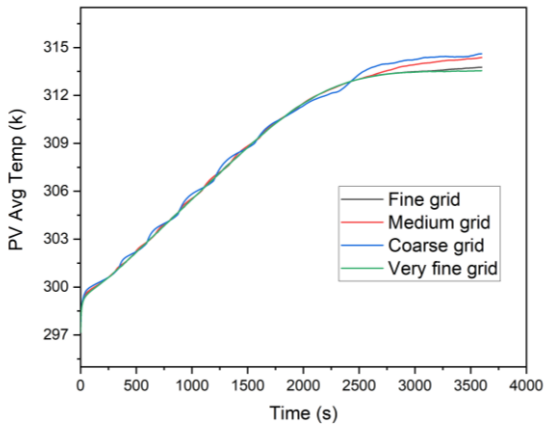

Figure 7: Mesh independence study.

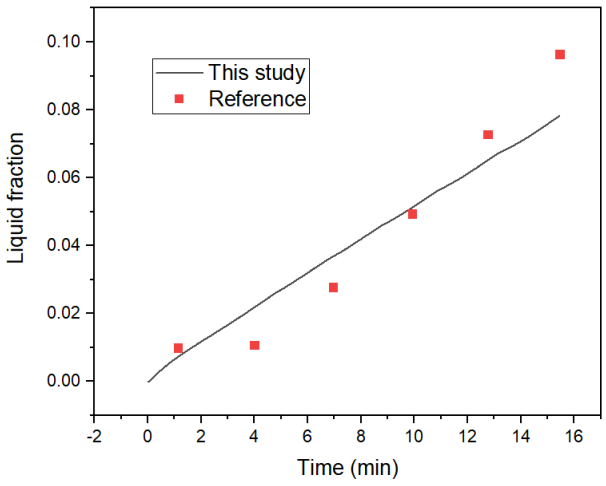

Figure 8: Model validation of liquid fraction variation with time.

NUST Journal of Engineering Sciences (NJES) is licensed under a Creative Commons Attribution 4.0 International License.

At later stages of melting, small deviations are seen. These differences can be attributed to differences in boundary-condition inputs, material-property inputs or numerical discretization schemes between the two studies. These small differences, despite the overall agreement, prove that the governing equations and phase change model that have been applied are properly formulated.

The close agreement between the simulated and reference results demonstrates the numerical model's reliability in capturing PCM melting behavior. Therefore, the model is reliable for studying thermal regulation in the proposed PV-PCM setup.

Parametric Analysis

In this section, the thermal response of the PV-PCM system in the presence of a constant solar heat flux of 1000 W/m2 is given. The discussion focuses on temperature development, phase-change development, and the overall performance of PCM implementation in managing module temperature. To clarify the discussion, the results are categorized into phases: heat absorption, behavior during melting, and comparative thermal performance.

Temperature Distribution in the PV–PCM System

Figure 9 shows the temperature contours at various time intervals. In the first stage, the whole system is in close contact with the ambient temperature (around 298 K), and heat conduction spreads through the layered structure. Solar absorption at the top surface increases the PV-layer temperature and creates a vertical thermal gradient toward the PCM.

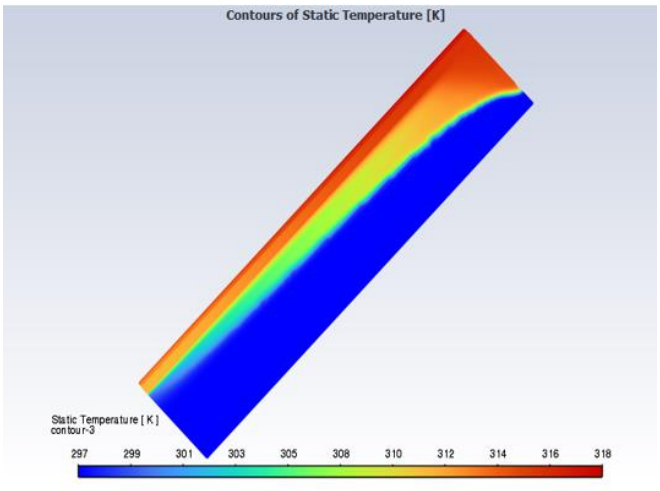

Figure 9: Contours of static temperature

The initial heating phase is characterized by high rates because the PCM is solid and accumulates energy as sensible heat. The temperature increase slows as the temperature approaches the melting point (RT25HC). This moderation is associated with latent heat absorption in the PCM layer.

The effect of noticeable temperature stabilization is realized when a phase transition occurs. Rather than rising steeply, the PV surface temperature increases more slowly. This implies that some of the heat flux entering the body is stored as latent heat rather than directly increasing the temperature.

Figure 10 shows the PV module's temporary temperature response. Three stages are evident:

1. First heating (0-1000 s): Typically, an almost linear increase in temperature, which is due to the absorption of sensible heat.
2. Active melting (1000-2500 s): The increase in temperature decreases because the absorption of latent heat of the phase change will moderate the PV surface temperature.
3. Post-melting (>2500 s): The temperature level becomes close to a quasi-steady state, latent heat capacity is practically depleted, sensible heat transfer occurs, and heat dissipation occurs.

The findings show that PCM integration can slow the temperature rise and improve temporary thermal control.

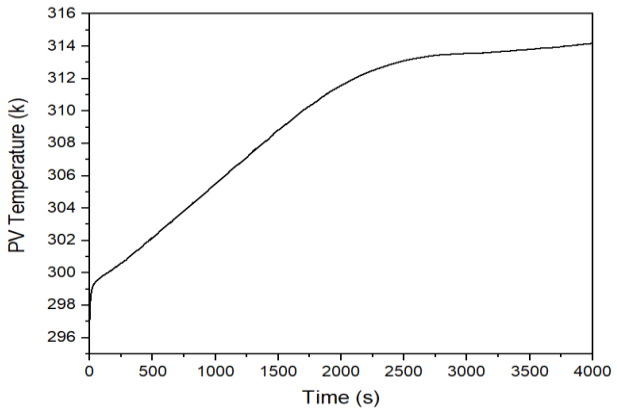

Figure 10: PV Panel temperature with PCM.

Liquid Fraction Evolution and Melting Behavior

Figure 11 shows the development of PCM liquid fraction. First, PCM is in a fully solid state ($\beta = 0$). When the interface temperature reaches the solidus point, local melting starts near the upper part of the aluminum layer.

However, over time, the melting front moves downward. Natural convection of the liquid fraction due to buoyancy causes an uneven distribution of the liquid fraction in the molten PCM. Warmer liquid rises, while comparatively cold regions remain at the bottom, resulting in uneven melting patterns.

This convective flow improves internal heat redistribution and increases the rate of phase transition compared with pure conduction. The fact that circulation cells are formed in the melted PCM is a testament to the fact that both conduction and natural convection play a role in the process of total heat transfer during the process of melting.

In the later phases, when the fraction of liquid is nearly equal to unity ($\beta = 1$), the system progressively returns to the situation where sensible heat storage is dominant again. As most of the PCM melts, the PV layer temperature starts climbing faster again, so the latent-heat buffering capacity decreases.

NUST Journal of Engineering Sciences (NJES) is licensed under a Creative Commons Attribution 4.0 International License.

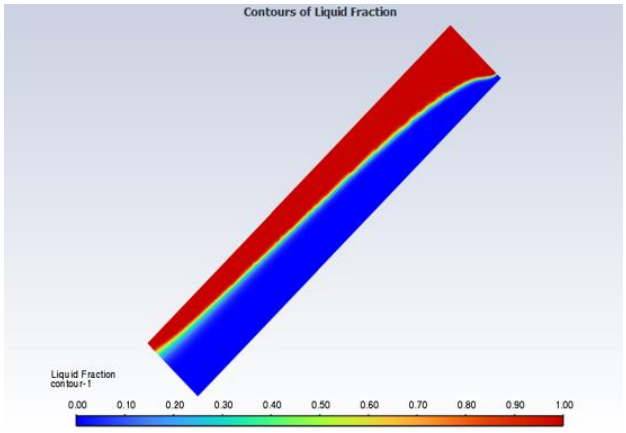

Figure 11: Contours of liquid fraction.

Figure 12 shows the time development of PCM liquid fraction. First, the PCM exists as a solid and absorbs energy as sensible heat. The liquid fraction rises gradually during melting and approaches unity when the PCM is fully melted. This continuous, smooth variation indicates numerical stability and the usefulness of PCM for thermal energy storage and temperature control.

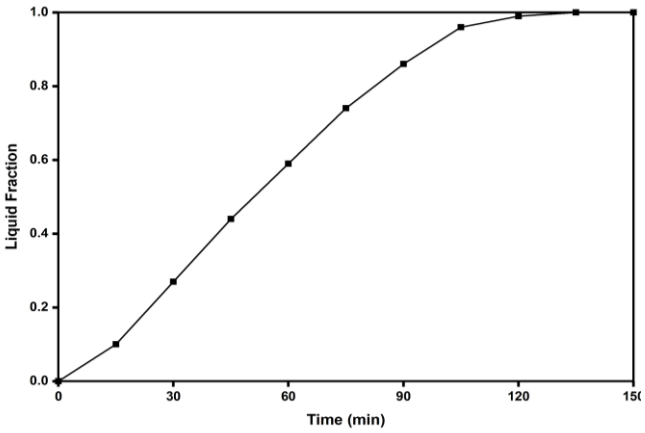

Figure 12: Liquid fraction of PCM variation with time

PCM Melting Behavior

The PCM liquid-fraction distribution during the melting process is illustrated in Figure 13. The figure shows the spatial development of the liquid region as heat is transferred from the PV module through the aluminum layer into the PCM. Initially, the PCM is predominantly solid, while melting begins in the region adjacent to the heated aluminum surface. As heating continues, the liquid region expands into the PCM layer. The non-uniform distribution of liquid fraction is associated with the coupled conduction and buoyancy-driven convection within the molten PCM.

These results demonstrate RT25HC's ability to absorb thermal energy through phase change and regulate the PV–PCM system's temperature rise. Since the present study does not provide a systematic set of simulations for multiple inclination angles, no quantitative conclusion regarding the effect of tilt angle is drawn here.

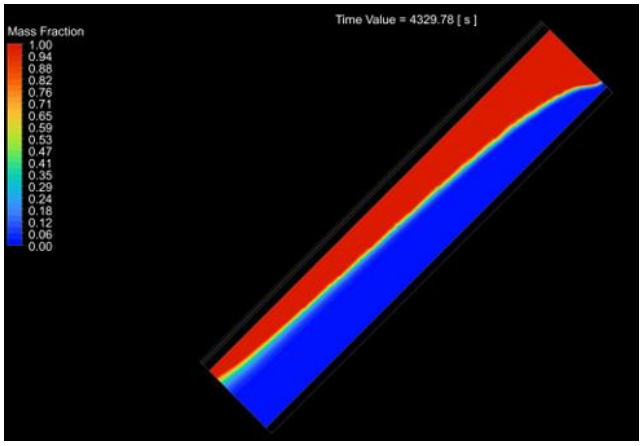

Figure 13: PCM liquid-fraction contour during the melting process.

Quantitative Comparison Between PV and PV–PCM Systems

To evaluate the efficiency of PCM integration, the thermal response of the PV–PCM system was compared to that of a standard PV module working in the same conditions (Table 4). Figure 14 indicates the temperature change in both arrangements. Without PCM, the PV module temperature increases sharply and reaches much higher peak values. The growth rate is high and steady because heat transfer depends on conduction only in the structural layers, in addition to natural convection at the outer surface. By contrast, the PV-PCM arrangement shows a more tempered temperature distribution. The peak PV temperature is reduced by about 33 K compared to the PV-only scenario. More importantly, the critical operating period shows a slower rate of temperature increase at the same solar intensity. This reduction in peak temperature directly affects electrical efficiency. PV efficiency also declines with cell temperature, so a narrower operating range improves performance. According to the simulated decrease in temperature, a potential increase in efficiency of close to 3 percent could be obtained.

Overall, PCM integration provides a passive, energy-neutral, and effective strategy for improving PV module thermal and electrical performance.

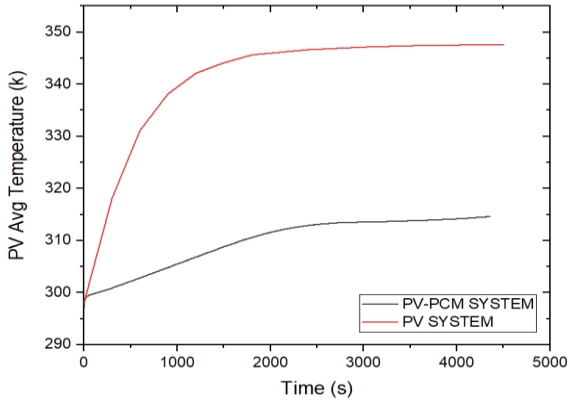

Figure 14: PV versus PV-PCM system temperature

NUST Journal of Engineering Sciences (NJES) is licensed under a Creative Commons Attribution 4.0 International License.

Table 4: Comparison of PV and PV-PCM System [23]

Parameter	PV-Only System	PV–PCM System
Initial PV Temperature	298 K	298 K
Maximum PV Temperature	348 K	315 K
Temperature Rise Rate	Rapid and steep	Slower and controlled
Thermal Stability	Lower (rapid overheating)	Higher (temperature-regulated)
Cooling Mechanism	Natural dissipation	Latent heat absorption via PCM
Heat Transfer Modes	Conduction + Convection	Conduction + Convection + Phase Change
Heat Storage Capacity	Low	High due to PCM latent heat
Peak Temperature Reduction	None	33 K reduction compared to PV-only
Electrical Efficiency	15.59 %	18.56 %
Absolute Efficiency Improvement	–	2.97 %
Relative Efficiency Improvement	–	~19.1%

Efficiency Analysis

The electrical efficiency of a photovoltaic module decreases as cell temperature increases. To measure the difference in performance between the PV-only and PV-PCM configuration, the temperature coefficient method was used with the normal empirical relationship:

$$\eta_T = \eta_{ref}\left[1 - \alpha(T - T_{ref})\right] \quad (16)$$

where, η_{ref} reference efficiency (20%) at usual test conditions (at $T_{ref} = 25^{o}$C), α is the temperature coefficient (0.0045°C -1 silicon PV), T is the cell temperature (°C) of the simulation results.

From the numerical simulations, the representative cell temperatures were:

- PV–PCM system: 315 K (41°C)
- PV-Only system: 348 K (74°C)

PV–PCM efficiency is calculated as;

$$\eta_{PCM} = 0.20[1 - 0.0045(41 - 25)]$$

$$\eta_{PCM} = 0.20(1 - 0.072)$$

$$\eta_{PCM} = 0.20 \times 0.928 = 18.56\%$$

PV-Only efficiency is calculated as;

$$\eta_{PV} = 0.20[1 - 0.0045(74 - 25)]$$

$$\eta_{PV} = 0.20(1 - 0.2205)$$

$$\eta_{PV} = 0.20 \times 0.7795 = 15.59\%$$

Introduction of PCM increased the estimated electrical efficiency from 15.59% for the PV-only configuration to 18.56% for the PV–PCM configuration. This corresponds to an absolute improvement of 2.97 percentage points and a relative improvement of approximately 19.1%. The improvement is attributed to the lower PV operating temperature resulting from thermal energy absorption by the PCM during melting. By limiting the PV cell temperature rise, the PCM reduces temperature-related electrical performance losses. These results suggest that thermal regulation using phase change materials not only regulates temperature but also provides electrical advantages measurable under high-irradiance conditions.

Conclusion

A two-dimensional transient CFD analysis was used to investigate the thermal characteristics of a photovoltaic cell coupled with RT25HC phase change material under sustained solar irradiation of 1000 W/m2. The numerical model that was used to describe both sensible and latent heat transfer in the PCM layer was simulated in ANSYS Fluent with the enthalpy-porosity method. The results indicate that RT25HC can regulate temperature rise during use. Latent heat absorption prevents further temperature increases as the module temperature approaches the melting range, driven by buoyancy-driven natural convection of the molten PCM. Compared with the PV-only configuration, the PV–PCM system reduced the maximum PV temperature from approximately 348 K to 315 K, corresponding to a reduction of about 33 K under the investigated operating condition. The estimated electrical efficiency increased from 15.59% to 18.56%, an absolute improvement of 2.97% and a relative improvement of approximately 19.1%. This improvement is mainly due to reduced performance degradation at low

NUST Journal of Engineering Sciences (NJES) is licensed under a Creative Commons Attribution 4.0 International License.

temperatures. Altogether, the analysis shows that incorporating a temperature-matched PCM like RT25HC provides passive, energy-neutral thermal management for photovoltaic modules. The results show the importance of choosing a PCM with a melting range consistent with anticipated operating temperatures, which leads to optimal functionality in warm climatic areas.

Acknowledgments
This research is supported by the U.S.-Pakistan Center for Advanced Studies in Energy, University of Engineering and Technology, Peshawar, Pakistan.

Competing Interests
None.

Authors' Contributions
M. Hassan: Conceptualization, methodology, project administration, review and supervision. M. E. Khan: Formal analysis, investigation, resources, data curation, software, visualization, writing the original draft, and writing, reviewing, and editing. M. S. Rehan and K. Ahmad: Validation, writing, review and editing.
All authors have read and agreed to the published version of the manuscript.

References

1. A. Ahmadi, M. E. H. Assad, D. H. Jamali, R. Kumar, Z. X. Li, T. Salameh*, et al.*, "Applications of geothermal organic Rankine Cycle for electricity production," *Journal of Cleaner Production,* vol. 274, p. 122950, 2020.
2. A. H. Alami, A. A. Hawili, M. Tawalbeh, R. Hasan, L. Al Mahmoud, S. Chibib*, et al.*, "Materials and logistics for carbon dioxide capture, storage and utilization," *Science of The Total Environment,* vol. 717, p. 137221, 2020.
3. C. Ghenai, T. Salameh, and A. Merabet, "Technico-economic analysis of off grid solar PV/Fuel cell energy system for residential community in desert region," *International Journal of Hydrogen Energy,* vol. 45, pp. 11460-11470, 2020.
4. A. Juaidi, F. G. Montoya, J. A. Gázquez, and F. Manzano-Agugliaro, "An overview of energy balance compared to sustainable energy in United Arab Emirates," *Renewable and sustainable energy Reviews,* vol. 55, pp. 1195-1209, 2016.
5. A. M. Al-Sabounchi, E. Al-Hammadi, S. Yalyali, and H. A. Al-Thani, "Photovoltaic-grid connection in the UAE: Technical perspective," *Renewable energy,* vol. 49, pp. 39-43, 2013.
6. S. A. M. Said, "Effects of dust accumulation on performances of thermal and photovoltaic flat-plate collectors," *Applied Energy,* vol. 37, pp. 73-84, 1990.
7. R. Siddiqui and U. Bajpai, "Deviation in the performance of solar module under climatic parameter as ambient temperature and wind velocity in composite climate," *International Journal of Renewable Energy Research,* vol. 2, pp. 486-490, 2012.
8. D. Connolly, H. Lund, B. V. Mathiesen, and M. Leahy, "A review of computer tools for analysing the integration of renewable energy into various energy systems," *Applied energy,* vol. 87, pp. 1059-1082, 2010.
9. R. Venkateswari and S. Sreejith, "Factors influencing the efficiency of photovoltaic system," *Renewable and Sustainable Energy Reviews,* vol. 101, pp. 376-394, 2019.
10. M. G. Chowdhury, D. Goossens, H. Goverde, and F. Catthoor, "Experimentally validated CFD simulations predicting wind effects on photovoltaic modules mounted on inclined surfaces," *Sustainable Energy Technologies and Assessments,* vol. 30, pp. 201-208, 2018.
11. D. C. Jordan, S. R. Kurtz, K. VanSant, and J. Newmiller, "Compendium of photovoltaic degradation rates," *Progress in Photovoltaics: Research and Applications,* vol. 24, pp. 978-989, 2016.
12. N. Dabaghzadeh and M. Eslami, "Temperature distribution in a photovoltaic module at various mounting and wind conditions: A complete CFD modeling," *Journal of Renewable and Sustainable Energy,* vol. 11, 2019.
13. C. M. Jubayer, K. Siddiqui, and H. Hangan, "CFD analysis of convective heat transfer from ground mounted solar panels," *Solar Energy,* vol. 133, pp. 556-566, 2016.
14. D. Ghosh and C. Guha, "Numerical simulation of paraffin wax melting in a rectangular cavity using CFD," *Indian Chemical Engineer,* vol. 62, pp. 314-328, 2020/07/02 2020.
15. D. Magare, O. Sastry, R. Gupta, B. Bora, Y. Singh, and H. Mohammed, "Wind effect modeling and analysis for estimation of photovoltaic module temperature," *Journal of Solar Energy Engineering,* vol. 140, p. 011008, 2018.
16. B. Rtimi, A. Benhmidene, and B. Chaouachi, "Effect of nanofluid flow in a rectangular heat exchanger on the performance of a photovoltaic panel," *Journal of Thermal Science and Engineering Applications,* vol. 14, p. 111005, 2022.
17. M. Shehram, M. N. Hamidi, A. A. Abdul Wahab, and M. K. Mat Desa, "Hybrid Solar Cooling Using Photovoltaic Panels and Graphene-Enhanced Phase Change Material Thermal Storage," *Journal of Thermal Science and Engineering Applications,* vol. 18, p. 021006, 2026.
18. A. Waqas, J. Ji, L. Xu, M. Ali, and J. Alvi, "Thermal and electrical management of photovoltaic panels using phase change materials–A review," *Renewable and Sustainable Energy Reviews,* vol. 92, pp. 254-271, 2018.
19. E. Cuce, T. Bali, and S. A. Sekucoglu, "Effects of passive cooling on performance of silicon photovoltaic cells," *International Journal of Low-Carbon Technologies,* vol. 6, pp. 299-308, 2011.
20. T. Ma, Z. Li, and J. Zhao, "Photovoltaic panel integrated with phase change materials (PV-PCM): technology

NUST Journal of Engineering Sciences (NJES) is licensed under a Creative Commons Attribution 4.0 International License.

overview and materials selection," *Renewable and Sustainable Energy Reviews,* vol. 116, p. 109406, 2019/12/01/ 2019.
21. C. Pagkalos, G. Dogkas, M. K. Koukou, J. Konstantaras, K. Lymperis, and M. G. Vrachopoulos, "Evaluation of water and paraffin PCM as storage media for use in thermal energy storage applications: A numerical approach," *International Journal of Thermofluids,* vol. 1, p. 100006, 2020.
22. A. K. Shukla, K. Sudhakar, and P. Baredar, "Simulation and performance analysis of 110 kWp grid-connected photovoltaic system for residential building in India: A comparative analysis of various PV technology," *Energy Reports,* vol. 2, pp. 82-88, 2016/11/01/ 2016.
23. M. E. Khan, "Numerical simulation of cooling for photovoltaic modules using phase change material," Master's Thesis, Thermal Systems Engineering, U.S.-Pakistan Center for Advanced Studies in Energy, University of Engineering and Technology Peshawar, Pakistan, 2026.
24. K. S. Unnikrishnan and B. Rohinikumar, "Three Dimensional Numerical Simulation of Effect of Inclination on the Performance of PV Module Integrated with PCM System," in *Fluid Mechanics and Fluid Power (Vol. 1)*, Singapore, 2023, pp. 409-415.



NUST Journal of Engineering Sciences (NJES) is licensed under a Creative Commons Attribution 4.0 International License.